Three-Dimensional Particle Simulations of Discharge Characteristics for a Miniature Microwave Discharge Ion Thruster Using Water as Propellant

IEPC-2017-241

Presented at the 35th International Electric Propulsion Conference
Georgia Institute of Technology • Atlanta, Georgia • USA
October 8 – 12, 2017

Kengo Nakamura[1]
Yokohama National University, Yokohama, Kanagawa, 240-8501, Japan

Hiroyuki Koizumi[2]
The University of Tokyo, Kashiwa, Chiba, 277-8561, Japan

and

Yoshinori Takao[3]
Yokohama National University, Yokohama, Kanagawa, 240-8501, Japan

Abstract: We have analyzed discharged characteristics of water for a miniature microwave discharge ion thruster using three-dimensional Particle-in-Cell simulations with Monte Carlo collisions. In this simulation, three ion species (H_2O^+, OH^+ and H^+) are taken into account. From the results, we find that ion density, potential and electron temperature are higher in ECR region near the antenna. For the ion composition ratio, H_2O^+ and OH^+ occupy more than 97%. However, H^+ occupies about 10% for ion current density and is not negligible for ion beam extraction. Then, in order to increase the extracted ion current, we propose difference propellant injection positions and have conducted three-dimensional Direct Simulations Monte Carlo method for neutral distributions. Injected from side of the thruster, high-density regions of neutral in the downstream of discharge chamber are formed. The results of discharge characteristics depending on neutral distributions will be presented at the conference.

Nomenclature

B_{ST}	=	magnetostatic field of permanent magnets
E_{EM}	=	microwave electromagnetic field
E_{ES}	=	electrostatic field
I_b	=	beam current
m	=	mass
P_{abs}	=	power absorbed in plasma
t	=	time
V_S	=	screen voltage
v	=	velocity
ε_0	=	vacuum permittivity

[1] Graduate Student, Department of Systems Integration, nakamura-kengo-bh@ynu.jp.
[2] Associate Professor, Department of Advanced Energy, koizumi@al.t.u-tokyo.ac.jp.
[3] Associate Professor, Division of Systems Research, takao@ynu.ac.jp.

ε_r = relative permittivity
η_{div} = efficiency of divergence
η_{mul} = efficiency of multiply charged ion
μ_0 = vacuum permeability
ρ = charge density
ϕ = electrostatic potential

I.Introduction

CUBESATS[1)] and microspacecrafts[2)] have seen unprecedented growth in recent years because the development costs and terms can be reduced for Earth observation and deep space exploration missions. In order to include propulsion system in CubeSat, researches and developments of propulsion systems such as electrospray thrusters[3)] and pulsed plasma thruster,[4)] which has simple structures and does not require high-pressure gas storage system, are conducted. However, ΔV of the satellite mounted them is not sufficient value for the missions. Then, Ion thrusters can be one of the candidates for a small and high-performance propulsion system. The research of a miniature ion propulsion system (MIPS) for 50-kg-class microspacecraft such as HODOYOSHI-4 was conducted in Japan, and its operation in space was successfully performed in 2014 for the first time in the world. The MIPS employs electron cyclotron resonance (ECR) discharges with ring-shaped permanent magnets for its ion source and neutralizer.[5-7)] It is necessary to be miniaturized further in order to mount propulsion system on 10-kg-class CubeSats. It is difficult to be miniaturized, however, since the MIPS utilizes xenon as the propellant so do the conventional ion thrusters, the high-pressure gas storage and feed system occupy most weight of the total propulsion system. To remove the gas storage system, a small ion thruster using water as a liquid propellant was proposed, and the preliminary ground operation of the thruster was already demonstrated by the University of Tokyo,[8)] while the details of the discharge characteristics are not well known yet. Since it is difficult to perform plasma diagnostics and to identify what ion species are dominant in a small discharge chamber, we have analyzed discharge characteristics of water using three-dimensional particle simulations in this study. Dependence on the absorbed power and influence of ionized ions are discussed.

Ion production cost of the current water ion thruster is not sufficient to meet a target value. In order to improve the ion production cost, it is necessary to further increase the extracted current. The distribution of plasma formed at the downstream of the discharge chamber is desirable due to the increase of extracted current. In our previous numerical model,[9)] we have analyzed discharge characteristics based on the assumption that the neutral distribution is uniform. On the other hand, in a small RF ion thruster (μN-RIT), by injecting propellant gas from the downstream, it leads to a better neutral gas supply in the outer ion production regions compared with injection from upstream.[10)] In this study, we have analyzed the neutral distribution in the discharge chamber of water ion thruster by using three-dimensional Direct Simulation Monte Carlo (DSMC) method for different injection positions. Furthermore, we have conducted three-dimensional Particle-in-Cell simulation with Monte Carlo collisions (PIC/MCC) method with the obtained neutral distribution to investigate the discharge characteristics, influence on the neutral distribution, and ion production cost. The results of discharge characteristics depending on neutral density will be shown in the conference.

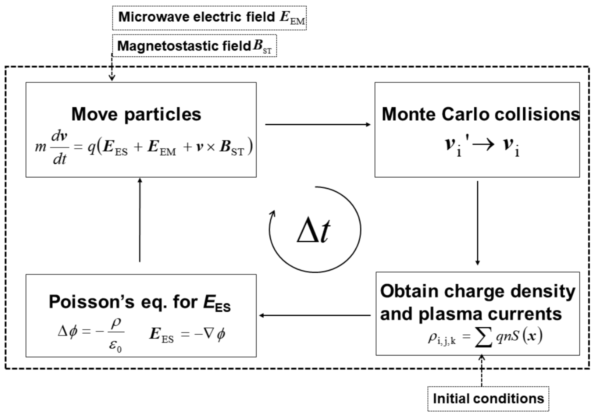

Figure 1. Calculation flow of the PIC/MCC simulation.

II.Numerical Model

The numerical methodology is basically the same as that employed in our previous paper,[11)] except for the propellant, grid spacing, and time step; and thus, the model is briefly described as below.

A. Configuration

Figure 1 shows the flowchart of the PIC/MCC simulation. We have employed a three-dimensional PIC/MCC method to analyze the kinetics of charged particles, together with finite-difference time-domain method (FDTD) for

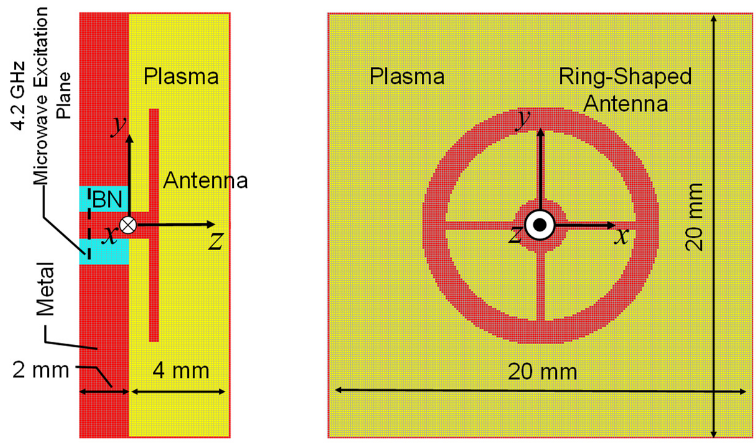

Figure 2. Schematic diagrams of the calculation model: (a) Side view (*z-y/x* plane at *x/y* = 0 mm) and (b) front view (*x-y* plane at *z* = 1.0 mm). In order to reduce calculation time, we have conducted the PIC/MCC simulation only for a quarter region using a point symmetry with respect to the *z*-axis.

the microwave elecrtomagnetic field $\boldsymbol{E}_{EM}$, and the finite element analysis using a software, ANSYS Emag™ for the magnetostatic field of the permanent magnets $\boldsymbol{B}_{ST}$.

Figure 2 shows the calculation model, where the size of the discharge chamber is 20 × 20 × 4 mm^3 with the ring-shaped antenna located at *z* = 1.0 mm. The inside of the coaxial waveguide is filled with the dielectric of boron nitride (BN). The 4.2 GHz microwave power is fed to the ring antenna through the four spokes. It should be noted that the BN region is also included in the electromagnetic field calculation of microwaves, although the PIC/MCC simulation area for the motion of charged particles is only the plasma region. In order to reduce the calculation time, we have conducted the simulation only for a quarter region of the calculation model as shown in Fig. 2. Figure 3 shows contour plots of the strength of the magnetic field of the ring-shaped permanent magnets at the *z-y* plane. The thick lines in red represent the resonant magnetic field of 0.15 T for 4.2 GHz microwaves.

Figure 4 shows the calculation model of the DSMC simulation. In order to simulate the propellant inflow, the metal region in Fig. 2 is expanded compared with PIC/MCC simulation area. In the DSMC simulation, we have analyzed for all regions. In order to consider the conditions under which the neutral density becomes high in the downstream of the discharge chamber, the propellant injection positions were considered the following positions of (a) the upstream, (b) downstream and (c) side (1 mm from the downstream), respectively. The detailed position conditions are as follows: (a) there are 8 injection ports with a diameter of 0.8 mm at a radius of 5.4 mm from center, (b) there are 4 injection ports with a diameter of 0.8 mm at 9 mm from the center, and (c) there are 4 injection ports with a length of 0.8 mm from side (*x* = 0 mm, *y* = 0 mm), respectively.

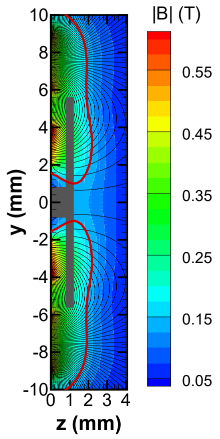

Figure 3. Contour plots at the *z-y* plane of the strength of the magnetic field, together with thick red lines in red representing the resonant magnetic field of 0.15 T for 4.2 GHz microwaves. (© IOP Publishing. Reproduced with permission. All rights reserved)[11]

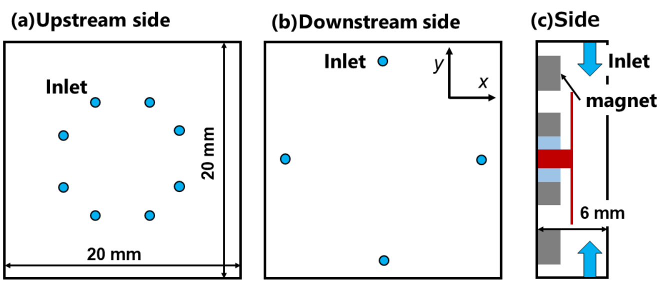

Figure 4. Calculation model of DSMC simulation, representing the injection position from (a) upstream side, (b) downstream side and (c) side.

B. Numerical Assumptions

The present PIC/MCC model has the following assumptions.

i) Singly-ionized water H_2O^+, hydroxide OH^+, hydrogen H^+, and electrons are treated as particles.
ii) Neutral particles are spatially and temporally uniform with a Maxwellian distribution at a gas temperature of 300 K in the plasma region.
iii) The magnetic fields of microwaves are negligibly small compared with the magnetostatic fields $\boldsymbol{B}_{ST}$.
iv) The motion of excited-state atoms is not considered.
v) Coulomb collisions are not taken into account.
vi) Since the power of microwaves is low in this simulation, the plasma current is neglected.[12)]

On the other hand, the present DSMC model has the following assumptions.

i) The gas is treated as a rarefied gas and a molecular flow since Knudsen number is more than 0.1.
ii) Considering the Knudsen number, rectilinear motion of the molecule and diffuse reflection on the wall are taken into account, and intermolecular collision is not taken into account.
iii) Since the intermolecular collision is not taken into consideration, it is difficult to simulate the flow in an inflow tube which is considered to cause many intermolecular collision, we have injected the particles from the injection port shown in Fig. 4.

C. Collisions

In electron-neutral collisions, the cross sections for the dominant reactions used in this analysis are shown in Fig. 5, where these are compiled from Itikawa and Nigel,[13)] Kawaguchi *et al.*,[14)] Yousfi and Benabdessadok,[15)] and Petro and Sedwick.[16)] In Fig. 5, excitation represents the sum of 26 types of the electronic excitations, which has a threshold energy of 7.14 eV. For a molecule like water, it is important to consider the energy dissipation mechanisms such as rotational and vibrational excitation collisions. In this analysis, rotational excitation at rotational transition J = 0→1–3 and vibrational excitation at stretching and bending mode are taken into account. In the ionized collisions, H_2O^+, OH^+, and H^+ are considered as ionized particles, since other ionized cross sections are small compared with these ionized species. Electron-neutral reactions used in this analysis are listed in Table 1. In ion-neutral collisions, only charge exchange collisions are taken into account.[17)]

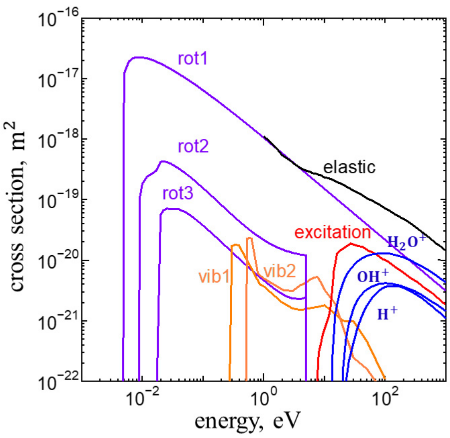

Figure 5. Electron-neutral collision cross sections of water vapor.

Table 1. Electron-neutral reactions of water considered in the present simulation.

Label	Type of collision	Reaction	Threshold energy, eV	Ref.
elastic	Elastic scattering	H_2O + e →H_2O + e		13)
rot1	Rotational excitation	H_2O (J = 0) + e →H_2O (J = 1) + e	4.60×10^{-3}	13, 14)
rot2	Rotational excitation	H_2O (J = 0) + e →H_2O (J = 2) + e	8.69×10^{-3}	13, 14)
rot3	Rotational excitation	H_2O (J = 0) + e →H_2O (J = 3) + e	1.18×10^{-2}	13, 14)
vib1	Vibrational excitation	H_2O (000) + e →H_2O (010) + e	0.198	13)
vib2	Vibrational excitation	H_2O (000) + e →H_2O [(100) + (001)] + e	0.453	13)
excitation	Electronic excitation	H_2O + e →H_2O^* + e	7.14	13)
H_2O^+	Ionization	H_2O + e →H_2O^+ + 2e	13.5	13)
OH^+	Ionization	H_2O + e →OH^+ + H + 2e	18.1	13)
H^+	Ionization	H_2O + e →H^+ + OH + 2e	16.9	13)

D. Additional Remarks

In this simulation, the grid spacing is set at 0.1 mm. The time step for FDTD is $\Delta t_{EM} = 1.49 \times 10^{-13}$ s (1/1600 of a microwave cycle for 4.2 GHz). The time steps for PIC/MCC are $\Delta t_e = 5.95 \times 10^{-12}$ s (1/40 of a microwave cycle) for electrons, and $\Delta t_i = 2.38 \times 10^{-10}$ s (one microwave cycle) for ions. The time steps for DSMC are $\Delta t_n = 3.87 \times 10^{-9}$ s.

Corresponding to a mass flow rate of at 35 μg/s in the experiment, [8)] the neutral pressure is set at 6.3 mTorr under uniform distribution conditions and neutral particles are injected accordingly in DSMC model.

III. Numerical Results and Discussion

Note that the distributions by PIC/MCC simulation shown in this paper are the results assumption that the distribution of neutral density is uniform.

A. Distributions of Plasma Parameters

Figures 6(a)–6(c) and 6(d)–6(f) show the distributions of the total ion density, the potential, and the electron temperature at the *z-y* plane for P_{abs} = 2.0 and 3.0 W, respectively. Here, the results are averaged over 30000 microwave cycles. For ion density at P_{abs} = 2.0 W in Fig. 6(a), since we found that a composition ratio of each ion is H_2O^+:OH^+:H^+ = 31:7:1, H_2O^+ is dominant for the ion species generated. This composition ratio is consistent with the ionized cross sections as shown in Fig. 5. From the composition ratio of the ion density, H_2O^+ and OH^+ densities occupy more than 97%. For the estimation of ion beam profiles there seems to be little adverse effect on thrust using water as the propellant because only a few lightweight H^+ is generated and the difference in molecular weight between H_2O^+ and OH^+ is just 1.0 g/mol; there would be almost no difference in ion beam trajectories between H_2O^+ and OH^+.

As the absorbed power increases, the maximal values of the ion density and the potential increase. On the other hand, the maximal value of the electron temperature almost remains unchanged, but the area of high electron

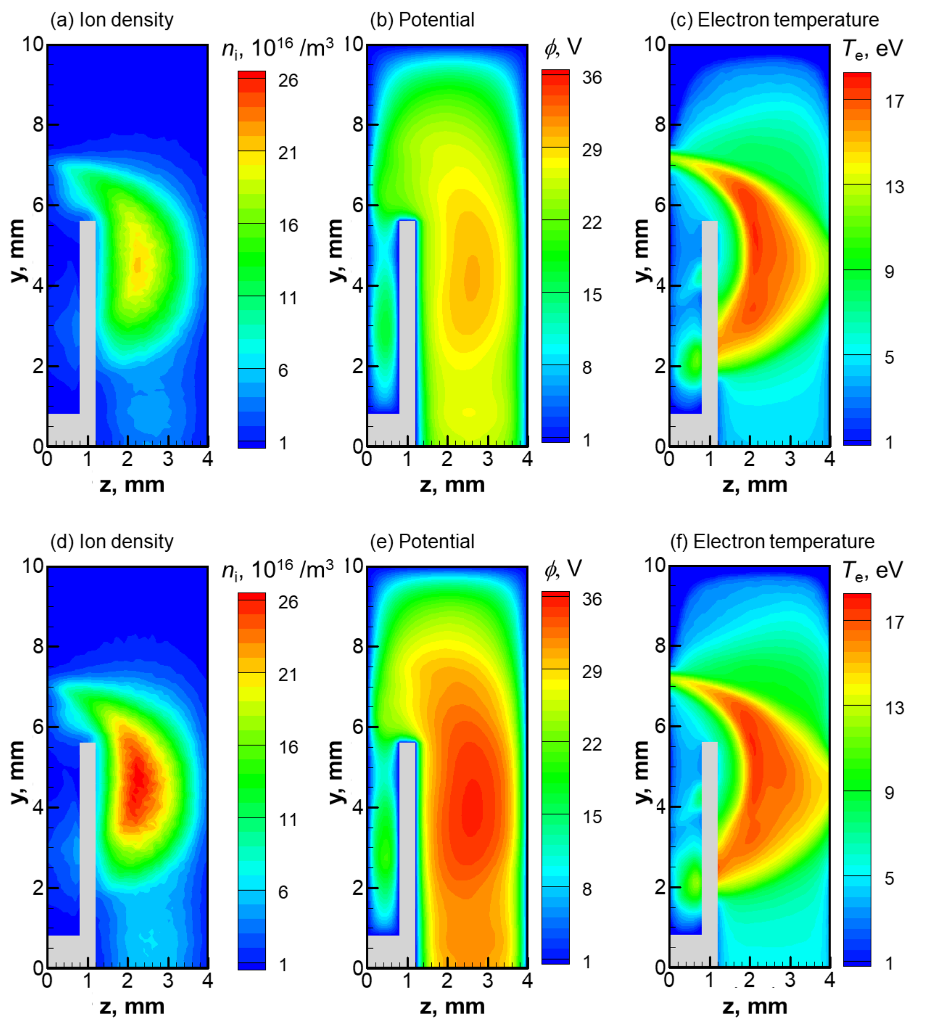

Figure 6. Plasma parameters contours at *z-y* plane at (a)-(c) P_{abs} = 2.0 W and (d)-(f) P_{abs} = 3.0 W.

temperature somewhat expands toward the downstream and central axis. Peak values of the ion density are located at z = 2.1–2.2 mm near the ECR region, and the electron temperature is higher than 17 eV at the area. Arcuate areas of the electron temperature more than about 13 eV are formed under both of power conditions. This is because that electrons move along the magnetic field (See Fig. 3) lines due to confinement by the mirror magnetic fields and the ionization reactions occur in the arcuate high temperature region since the threshold energy of ionization is 13.5 eV. The plasma confinement results in the distribution of the plasma density as shown in Figs. 6(a) and 6(d). However, all the electrons cannot be confined by the mirror magnetic field; some electrons of high energy are lost through a loss cone. Hence, increasing the absorbed power expands the area of high electron temperature and does not increase its peak value, as you can see from Figs. 6(c) and 6(f).

B. Ion Current Density

We consider effects of ion species on the thrust. The thrust for ion thruster is estimated with Eq. (1)

$$F = \eta_{\mathrm{mul}}\eta_{\mathrm{div}}\sqrt{\frac{2m_{\mathrm{i}}V_{\mathrm{S}}}{q}}I_{\mathrm{b}}. \qquad (1)$$

For the water propellant, Eq. (1) indicates that m_{i} affects the thrust since various ions are generated so that the effect of each ion species was investigated. Figure 7 shows the distributions of the ion current density for H_2O^+, OH^+, and H^+ in the z-direction for P_{abs} = 2.0 W at the z-y plane (x = 0 mm). As you can see, the direction of j_z changed at around

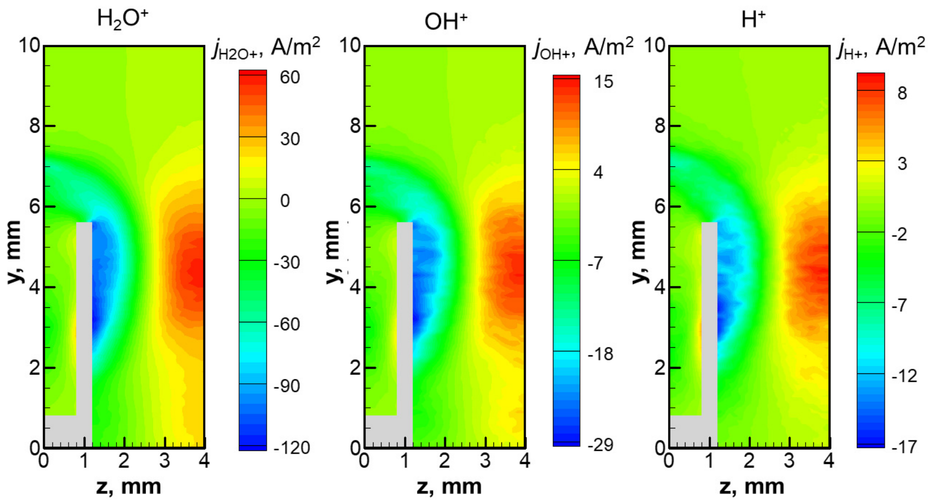

Figure 7. Ion current density contours at z-y plane at P_{abs} = 2.0 W for H_2O^+, OH^+ and H^+, respectively.

z = 2.6 mm, and almost all of ions are lost on the wall at z = 4.0 mm and the antenna. It should be noted that j_z at z = 4.0 mm spreads over the entire area of the x-y plane although j_z in the negative z-direction is concentrated on the ring-shaped antenna and its four spokes shown in Fig. 2. This configuration results in the larger absolute value of the negative j_z. At z = 4.0 mm, the ion current density becomes the highest at the region where the highest ion number density in x-y plane is obtained. Although we have not considered extraction of ions in this analysis, the averaged values of ion current density at z = 4.0 mm, which is an estimation of the thrust, are shown in Table 2. These values are averaged between 0 and 7.0 mm in the x and y directions since the ion current flowing into those areas mainly contributes to the thrust. Table 2 indicates that the ion current density of H_2O^+ is the largest among the ion species examined. Moreover, the ion current density of H^+ occupies about 10% of the total ion current density. Comparing the ion number density and the ion current density, the ratio of H^+ current density increases owing to the high speed of lightweight H^+, and its contribution for thrust cannot be neglected although the number density of H^+ is smaller than 3%. This result implies that the discharge condition to reduce the H^+ current density should be investigated or the grid system fit for both heavy H_2O^+, OH^+ and light H^+ is required.

Table 2. The averaged value of ion current density for each ion species at z = 4.0 mm.

Ion species	J_z averaged at z = 4.0 mm
H_2O^+	30.8 A/m²
OH^+	7.02 A/m²
H^+	4.08 A/m²

C. Distributions of Neutral Density

The distribution of neutral density at *z-y* plane in PIC/MCC calculation region are shown in Fig. 8. The reason why the distributions appear sparsely is due to the large weight (10^9) of superparticle. Injected from the upstream, the distribution of neutral density on the upstream face of the antenna is higher than that on the downstream face. The result is caused by the reflection of many particles on the antenna surface. Injected from the downstream and the side, the neutral density near the injection position is higher than other regions. Considering the ionization region from the distribution of electron temperature in Figs. 6(c) and 6(f), increasing plasma density in the downstream of discharge chamber cannot be expected injected from downstream. On the other hand, injected from the side, it can be expected to increase plasma density. This is because high-neutral density distribution is formed toward the central axis. The results of discharge characteristics depending on neutral distribution will be presented at the conference.

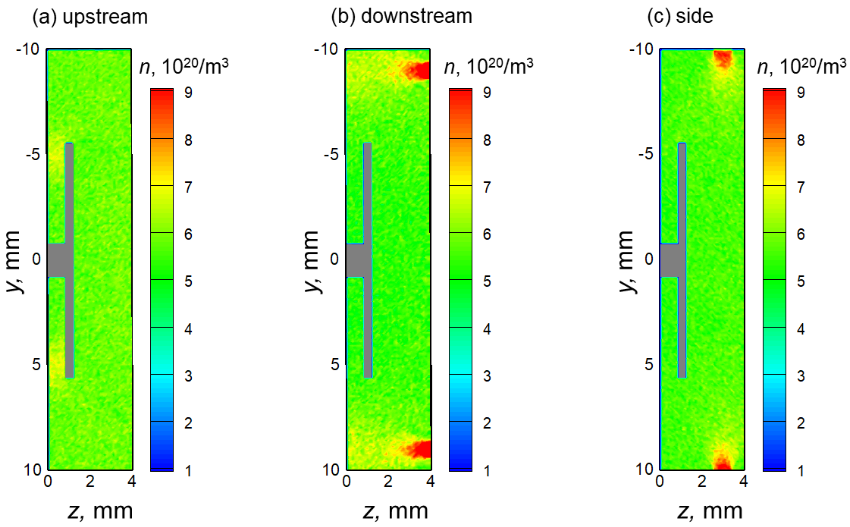

Figure 8. Time-averaged distributions of neutral density injected from (a) upstream, (b) downstream and (c) side in PIC/MCC calculation region.

IV.Conclusion

In this study, we have analyzed the discharge characteristics of water, which is employed as the propellant of a miniature microwave discharge ion thruster, using three-dimensional particle simulations (PIC/MCC), where three ion species (H_2O^+, OH^+, and H^+) are considered. PIC/MCC results that H_2O^+ and OH^+ densities occupy more than 97% for the ion density. Furthermore, ion density, potential and electron temperature have maximal values in the ECR region near the antenna. Although the number density of H^+ is smaller than 3%, the current density of H^+ exceeds 10% and thus, the effect of H^+ would not be negligible for ion beam extraction. DSMC results indicate that increasing ionization reaction in the downstream of discharge chamber is expected by injecting propellant from the side of the thruster. We have analyzed discharge characteristics depending on neural distribution using by PIC/MCC and will be presented the results at the conference.

In future work, in order to improve the ion production cost, we will optimize the propellant injection position and analyze the discharge characteristics depending on neutral density. Moreover, negative ion species, such as OH^-, H^- and O^- will also be considered in an improved model.

Acknowledgments

This work was supported in part by JSPS KAKENHI Grant Number JP16H06370. Part of the computer simulation was performed on the KDK computer system at Research Institute for Sustainable Humanosphere, Kyoto University.

References

[1] NASA JPL, "Mars Cube One (Marco) Mission Overview," URL: http://www.jpl.nasa.gov/cubesat/missions/marco.php [cited 18 September 2017].

[2]Koizumi, H., Kawahara, H., Yaginuma, K., Asakawa, J., Nakagawa, Y., Nakamura, Y., Kojima, S., Matsuguma, T., Funase, R., Nakatsuka, J., and Komurasaki, K., "Initial Flight Operations of the Miniature Propulsion System Installed on Small Space Probe: PROCYON," *Transactions of Japan Society for Aeronautical and Space Sciences, Aerospace Tech. Japan*, Vol. 14, No. ists 30, 2016, pp. Pb_13-Pb_22.

[3]Nakagawa, K., Tsuchiya, T., and Takao, Y., "Microfabricated emitter array for an ionic liquid electrospray thruster," *Japanese Journal of Applied Physics,* Vol. 56, No. 6S1, 2017, 06GN18.

[4]Rayburn, C., Campbell, M., and Mattick, A., "Pulsed Plasma Thruster System for Microsatellites," *Journal of Spacecraft and Rockets,* Vol. 42, No. 1, 2005, pp. 161-170.

[5]Kuninaka, H., Nishiyama, K., Funaki, I., Yamada, T., Shimizu, Y., and Kawaguchi, J., "Powered Flight of Electron Cyclotron Resonance Ion Engines on Hayabusa Explorer," *Journal of Propulsion and Power*, Vol. 23, No. 3, 2007, pp. 544-551.

[6]Kuninaka, H. and Satori, S., "Development and Demonstration of a Cathodeless Electron Cyclotron Resonance Ion Thruster," *Journal of Propulsion and Power.*, Vol. 14, No. 6, 1998, pp. 1022-1026.

[7]Koizumi, H. and Kuninaka, H., "Miniature Microwave Discharge Ion Thruster Driven by 1 Watt Microwave Power," *Journal of Propulsion and Power.*, Vol. 26, No. 3, 2010, pp. 601-604.

[8] Nakagawa, Y., Kawahara, H., Koizumi, H., and Komurasaki, K., "Fundamental Experiments with Liquid Propellants for the Microwave-discharge Ion Thruster," *Proceedings of Space Propulsion 2016*, 2016, SP2016-312540.

[9]Nakamura, K., Koizumi, H., and Takao, Y., "Numerical Analysis of a Miniature Microwave Discharge Ion Thruster Using Water as Propellant," *Proceedings of the 31st International Symposium on Technology and Science*, 2017, ISTS-2017-b-23.

[10]Henrich, R., Feili, D., and Heiliger, C., "Self-consistent Simulation of the Coupling Between Plasma and Neutral Gas in μN-RIT," *Proceedings of the 32nd International Electric Propulsion Conference*, 2011, IEPC-2011-323.

[11]Takao, Y., Koizumi, H., Komurasaki, K., Eriguchi, K., and Ono, K., "Three-dimensional particle-in-cell simulation of a miniature plasma source for a microwave discharge ion thruster," *Plasma Sources Science and Technology*, Vol. 23, No. 6, 2014, pp. 064004-1-11.

[12]Takao, Y., Eriguchi, K., Ono, K., Sugita, Y., Koizumi, H., and Komurasaki, K., "A Validation Study of a 3D PIC Model for a Miniature Microwave Discharge Ion Thruster," *Proceedings of the 50th AIAA/ASME/SAE/ASEE Joint Propulsion Conf*erence, 2014, AIAA-2014-3829.

[13]Itikawa, Y. and Nigel, M., "Cross Sections for Electron Collisions with Water Molecules," *Journal of Physical Chemistry,* Vol. 34, No. 1, 2005, pp. 1-22.

[14]Kawaguchi, S., Takahashi, K., Satori, K., and Itoh, H., "Electron transport analysis in water vapor," *Japanese Journal of Applied Physics,* Vol. 55, No. 7S2, 2016, pp. 07LD03-1-7.

[15]Yousfi, M. and Benabdessadok, M.D., "Boltzman equation analysis of electron-molecule collision cross sections in water vapor and ammonia," *Journal of Applied Physics*, Vol. 80, No. 12, 1996, pp. 6619-6630.

[16]Petro, E. M. and Sedwick, R. J., "Effects of Water-Vapor Propellant on Electrodeless Thruster Performance," *Journal of Propulsion and Power* (Article in Advance).

[17]Lishawa, C. R., Dressler, R. A., Gardner, J. A., Salter, R. H. and Murad, E., "Cross sections and product kinetic energy analysis of $H2O^+$–H2O collisions at suprathermal energies," *Journal of Chemical Physics,* Vol. 93, No. 5,1990, pp. 3196-3206.